ADVANCED MATERIALS

www.advmat.de

Hierarchical Graphene Foam for Efficient Omnidirectional Solar–Thermal Energy Conversion

Huaying Ren, Miao Tang, Baolu Guan, Kexin Wang, Jiawei Yang, Feifan Wang, Mingzhan Wang, Jingyuan Shan, Zhaolong Chen, Di Wei, Hailin Peng, and Zhongfan Liu**

Efficient solar–thermal energy conversion is essential for the harvesting and transformation of abundant solar energy, leading to the exploration and design of efficient solar–thermal materials. Carbon-based materials, especially graphene, have the advantages of broadband absorption and excellent photothermal properties, and hold promise for solar–thermal energy conversion. However, to date, graphene-based solar–thermal materials with superior omnidirectional light harvesting performances remain elusive. Herein, hierarchical graphene foam (h-G foam) with continuous porosity grown via plasma-enhanced chemical vapor deposition is reported, showing dramatic enhancement of broadband and omnidirectional absorption of sunlight, which thereby can enable a considerable elevation of temperature. Used as a heating material, the external solar–thermal energy conversion efficiency of the h-G foam impressively reaches up to ≈93.4%, and the solar–vapor conversion efficiency exceeds 90% for seawater desalination with high endurance.

Efficient conversion and exploitation of abundant solar energy are critically significant to meet the ever-growing global demands of inexhaustible and ecofriendly energy. Solar–thermal energy conversion is an essential step to that end. For example, many applications such as solar–thermal power generation, household water heaters, phase separation, and water purification/desalination are based on the conversion of sunlight to heat. So far, a variety of emerging photothermal materials have been explored, including metallic nanoparticles,[1–3] metal-salts/oxides,[4,5] and carbon-based materials.[6–8] With electrons excited on resonance, the temperature around metallic nanoparticles such as Au will rise drastically. The localized heating effect makes them good solar–thermal conversion material. However, to increase the conversion efficiency, these metallic nanoparticles usually need cumbersome morphology regulation to overcome their inherently narrow absorption bandwidth; and, most often, the metallic-based materials are far from stable in corrosive media like acid, alkali, and salt, which limits the long-term usage of these materials.

Owing to the broadband absorption nature[9] and excellent chemical stability, carbon-based materials such as carbon nanotubes and graphene stand out as photothermal materials in extensive studies, such as photothermal therapy,[10,11] environmental remediation,[12] and solar–steam generation[6,7,13,14] for water purification/desalination. Nevertheless, to pragmatically achieve an efficient solar–vapor conversion, these carbon-based solar–thermal materials still need to be improved in the following aspects: i) a facile preparation process and high production output; ii) efficient omnidirectional absorption of sunlight with less transmittance and reflectance; iii) a larger contact area between the material and the matrix for better heat and mass transfer. A rational porous structure with an increased surface area is well suited to provide a sufficient heat exchange contact. Some preparation methods of porous graphene foams were reported by chemical vapor deposition.[15–19] However, conventional few-layered graphene foams suffer from the relatively flat surface at the microscale, resulting in limited absorption and relatively high light reflection, which deteriorated the overall efficiency. This limit can be overcome by increasing the light–matter interaction length[20] and absorption times in vertical graphene sheets[21] of the hierarchical foam.

In this paper, the hierarchical foam of graphene was designed and synthesized via a facile one-step plasma-enhanced chemical vapor deposition (PECVD) growth method. The foam is utilized as an efficient solar–thermal conversion medium. It consists of vertical graphene nanoplates (GNPs) array on the

H. Ren, M. Tang, K. Wang, F. Wang, M. Wang, J. Shan, Z. Chen, Prof. H. Peng, Prof. Z. Liu
Center for Nanochemistry
Beijing Science and Engineering Center for Nanocarbons
Beijing National Laboratory for Molecular Sciences (BNLMS)
College of Chemistry and Molecular Engineering
Peking University
Beijing 100871, P. R. China
E-mail: hlpeng@pku.edu.cn; zfliu@pku.edu.cn
H. Ren, J. Shan
Academy for Advanced Interdisciplinary Studies
Peking University
Beijing 100871, P. R. China
Prof. B. Guan, J. Yang
Key Laboratory of Opto-Electronics Technology
Ministry of Education
College of Electronic Science and Technology
Faculty of Information Technology
Beijing University of Technology
Beijing 100022, P. R. China
Dr. D. Wei
Beijing Graphene Institute
Beijing 100094, P. R. China

DOI: 10.1002/adma.201702590

3D foam skeleton, which provides a much larger heat exchange area. Optically, such a unique structure guarantees the high solar spectrum absorption at an arbitrary incident angle with decreased reflection, leading to a considerable enhancement to the temperature rise. The solar–thermal experiments showed that the external solar–thermal conversion efficiency of the h-G foam reached ≈93.4%, which outperforms the majority of the conventional solar–thermal materials. Furthermore, the h-G foam is also endowed with outstanding corrosion stability and lightweight, which makes it an ideal portable solar–thermal material for applications such as waste water treatment and seawater desalination. Portable desalination system using h-G foam was carefully explored with an excellent efficiency (solar–vapor conversion efficiency ≈91.4%), long durability and recycling performance.

Compared to ordinary graphene foam (G foam), the designed h-G foam consists of secondary structures (**Figure 1**a), i.e., the GNPs secondary structure anchored on the 3D skeleton primary structure inherited from the porous substrate (detailed in Figure S1a, Supporting Information). This h-G foam could minimize the reflection and transmission of incident light to convert the absorbed light to heat effectively. A scalable one-step growth method was developed to prepare the designed material by PECVD using nickel foam (Ni foam) as the substrate at a relatively low temperature of 700 °C. Methane was chosen as the precursor considering the high atomic hydrogen to carbon ratio, which is critical to the GNPs growth by keeping atomically thin and reducing the defects.[22,23] 50 cm^2 h-G foam was obtained, which is flexible (Figure 1b) and ultralight (2.8 mg cm^{-3}) after removing the substrate. Scanning electron microscopy (SEM) images clearly show that as-synthesized h-G foam comprises of primary structure (Figure 1c) and secondary structure of GNPs with random orientations (Figure 1d and Figure S1b,c, Supporting Information). The transmission electron microscopy (TEM) observation further corroborates its hierarchical structure (Figure 1e). The average thickness of each palate is around 3–5 nm (Figure 1e bottom inset), namely 9–15 layers of graphene, while the average length of GNP can be controlled by the growth time until they reach 400 nm (Details discussed in Figure S2, Supporting Information). Notably, the nucleation density remains unchanged during the growth process, which indicates the nanoplates are all grown from primary nucleation. Raman spectra were measured to further characterize the quality of the h-G foam with different GNP length. In detail, intensity of the 2D peaks (≈2690 cm^{-1}) is 0.64–0.80 times greater than that of G peaks (≈1580 cm^{-1}) and I_D/I_G decreases

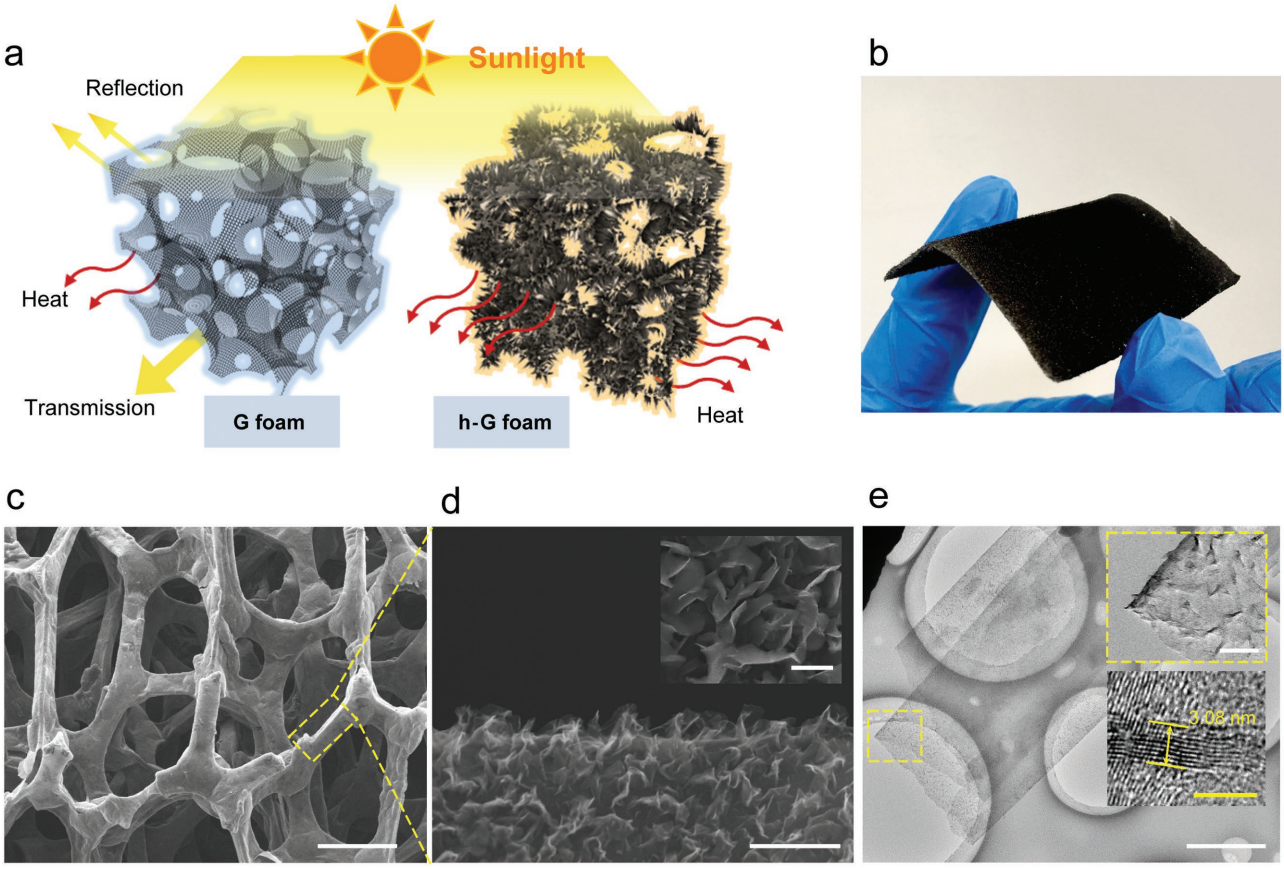

Figure 1. Structure and controlled growth of hierarchical graphene foam. a) A schematic of solar–thermal conversion difference between ordinary graphene foam and h-G foam. b) Optical image of flexible h-G foam. c) SEM image of the h-G foam in low magnification. Scale bar: 200 µm. d) SEM image of the frame edge, inset: top view of the frame. Scale bar in (d) and (d inset): 500 and 200 nm. e) Typical TEM images of h-G foam. The bottom inset is high resolution TEM image, showing the thickness of the vertical graphene GNP about 3.08 nm (nine layered). The top inset is partial enlarged view of h-G foam, corresponding to the yellow dashed box. Scale bars in (e): 500 nm; scale bar in top inset of (e): 100 nm; scale bar in bottom inset of (e): 5 nm.

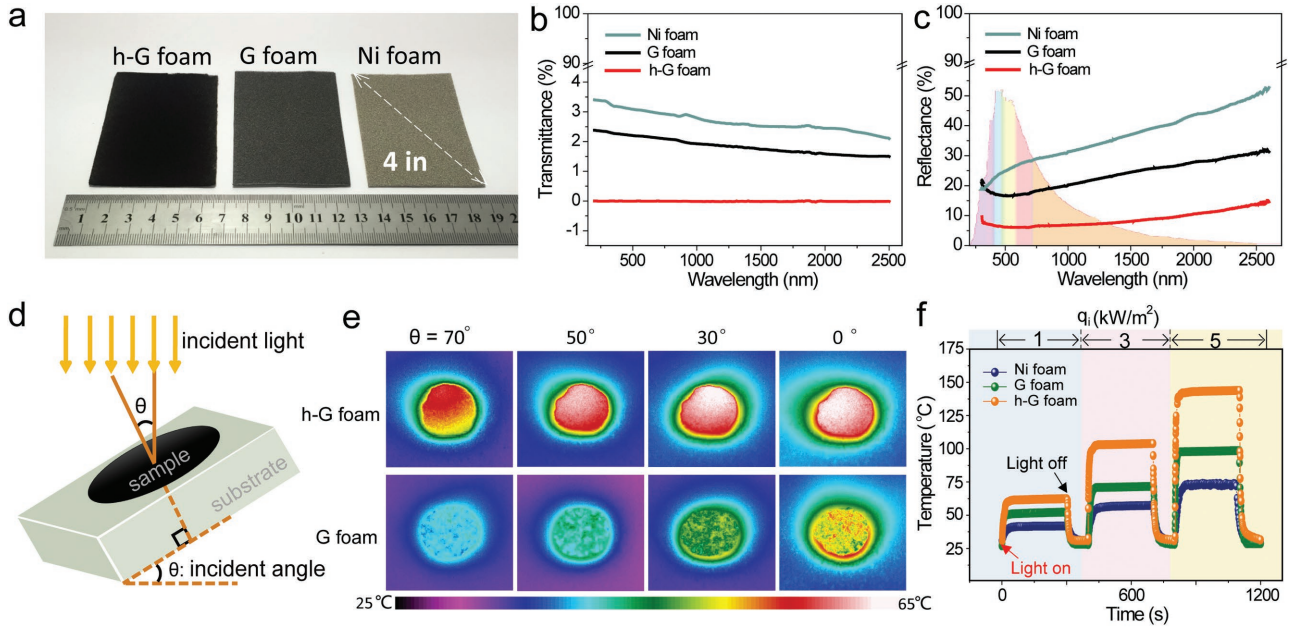

Figure 2. Light absorption and heat conversion of h-G foam. a) Optical image of h-G foam, G foam, and nickel foam. b,c) Transmittance and diffuse reflectance spectra of h-G foam (red), G foam (black), and nickel foam (olive). The background of colorized region represents the solar spectrum. d) Schematic of the incident angle. e) IR image of h-G foam and G foam at varied incident angles (70°, 50°, 30°, and 0°) after reaching temperature stable state under q_i = 1 kW m^{-2}. f) The temperature changing course of h-G foam (orange), G foam (green), and nickel foam (blue) under solar illumination of q_i = 1, 3, 5 kW m^{-2} on and off.

with the length of the GNP, implying better quality of h-G foam with longer GNPs[24] (shown in Figure S3, Supporting Information).

Figure 2a contrasts the color difference of h-G foam, ordinary graphene foam, and Ni foam, among which h-G foam is the blackest one. It demonstrates the absorption of h-G foam within visible wavelengths is dramatically enhanced by its hierarchical structure. The diffuse reflectance and transmission spectra further indicate its broadband adsorption property (Figure 2b,c) (range of solar irradiance spectrum at Earth's surface: 295–2500 nm). Remarkably, the h-G foam shows the lowest transmittance (≈0%) and reflectance (≈5% at visible region, ≈10% at near infrared region, and <15% higher in infrared region), which is superior to G foam and Ni foam. The results imply that the light may be "trapped" within the material and absorbed vastly instead of bouncing off or penetrating the h-G foam (as schematically shown in Figure 1a), evincing the advantages of the h-G foam for the maximization of the light collection.

Considering the various positions of the sun in reality, less dependence on the light incoming direction is also a fundamental requirement of solar energy utilization. Surface temperatures of different samples under 1 kW m^{-2} light with varied incident angles were measured (shown in Figure 2d and setup see Figure S6, Supporting Information). Compared to G foam, h-G foam performs good solar–thermal conversion stability as the incident angle increases from 0° to 50° (Figure 2e). At large angle of 70° the temperature seems declined a little (around 55 °C for h-G foam), which is caused by the sharply reduced projected area. A photocalorimetric study was performed by illuminating the materials (h-G foam, G foam, and Ni foam) in the same shape and size. With the radiation power of the solar illumination elevated from 1 to 5 kW m^{-2}, the surface temperature change (ΔT) of h-G foam increased from 33.5 to 114.8 °C (Figure 2f). For G foam and Ni foam in parallel tests, the ΔT_s are 23.4–69.5 and 12.8–43.8 °C, respectively. These conspicuous differences in the change of temperature are readily visualized by infrared images (Figure S5, Supporting Information), showing the outstanding photothermal property of h-G foam. The solar–thermal conversion efficiency η_{st} of h-G foam was calculated from the thermal profile of Figure 2f to be 93.4% ± 3% via the energy balance function[5,25,26]

$$m_i C_{p,i} \frac{dT}{dt} = \dot{Q}_{in} - \dot{Q}_{surr,out} \quad (1)$$

where m_i and $C_{p,i}$ are the mass and heat capacity of material, and $\dot{Q}_{in}$ and $\dot{Q}_{surr,out}$ are the heat input per unit time from the material and heat dissipation per unit time to the surrounding (detailed derivation in the Supporting Information). The efficiency of the h-G foam is superior to other state of art carbon-based materials like exfoliated graphite[7] (56–66%) and porous graphene foam[8] (46–80%). To sum up, in spite of the weaken solar–thermal capability under very large incident angles, the h-G foam shows prominent solar–thermal effect in all cases due to the high omnidirectional light absorption efficiency with broadband spectrum ranges.

The light absorption enhancement is directly associated with the microstructure of the h-G foam. This can be easily understood that first, light-matter interaction length is longer when GNPs were along the direction of incident light.[20] Second, light is reflected away partly on relatively flat surface

(Figure S7a, Supporting Information). However, on the GNPs anchored surface the light gets trapped in the gaps resulting in multiple internal reflections until absorbed completely (Figure S7a,b, Supporting Information).[26] In addition, the nanoplates' dimensions (100–400 nm) are smaller than most part of the wavelength of solar spectrum. If the distances between the GNPs are appropriate, light would interact differently on the GNPs structures due to the equivalent gradient refractive index.[26] Electromagnetic simulations using finite difference time domain were carried out to simulate the light absorption in a cell section extracted from h-G foam 3D skeleton. In the model presented in this paper, the squared GNPs (100 nm in length and ten layered graphene) were sitting on the few-layered graphene film. The absorbance of the film with GNP is increased along with the increasing incident angle (0° to 50°). In contrast, under the same incident condition the absorbance of graphene film without GNP becomes weaker (**Figure 3**a inset). As a result, the absorbance per-unit projected area (absorbance multiply by cos θ) is almost unchanged along with the increasing incident angle (Figure 3a), well explaining the omnidirectional solar–thermal performance of the h-G foam. It is noted that the petal-like GNPs are randomly orientated having 45°–90° angles with the skeleton surface (Figure S1b,c, Supporting Information). But to simplify the microstructure modeling, graphene plates with two typical angles, 45° and 90° were selected in contrast with the few-layered graphene without GNP (Figure 3b inset). The simulated absorption curves of GNPs with angle of 45°, 90° and without GNP on few-layered graphene reveal that the GNPs play very important role in enhancing the absorption (Figure 3b). Both reflectance and transmittance of GNP 45° and GNP 90° are reduced compared to those of graphene film (Figure S8a,b, Supporting Information). The reflectance decreased mainly in UV–vis ranges (the most energetic part of the solar spectrum), while the transmittance reduction covers the whole range of solar spectrum. Moreover, to elucidate the absorption enhancement visually, the calculated cross-sectional electric field distributions of the three models at wavelength of 600 (Figure 3c–e) and 1500 nm (Figure S8c–e, Supporting Information) were presented. For pure few-layered graphene, the absorbance is small in the visible range. However, this small absorbance together with GNPs absorbance in the infrared regime throughout the volume of the sunlight causes an ≈16% electric field intensity decrease in steady-state condition. The absorption enhancement of cell section of the h-foam is obvious, the total absorption of the whole foam will further increase due to the multiple interaction between light and the 3D network (i.e., numerous replicates of the simulated model), which will lead to enhanced temperature rise compared with ordinary graphene foam.

Considering the outstanding solar–thermal properties and bicontinuous hierarchical foam structure of h-G foam, the performances of solar–vapor conversion and desalination application were experimentally studied. A sectional typed solar–vapor desalination unit composed of collection cap and steam generation chamber was designed, as illustrated in **Figure 4**a. The h-G foam was placed on the surface of the liquid as the solar driven localized heater to vaporize the water on the top (Movie S1, Supporting Information). A dramatic

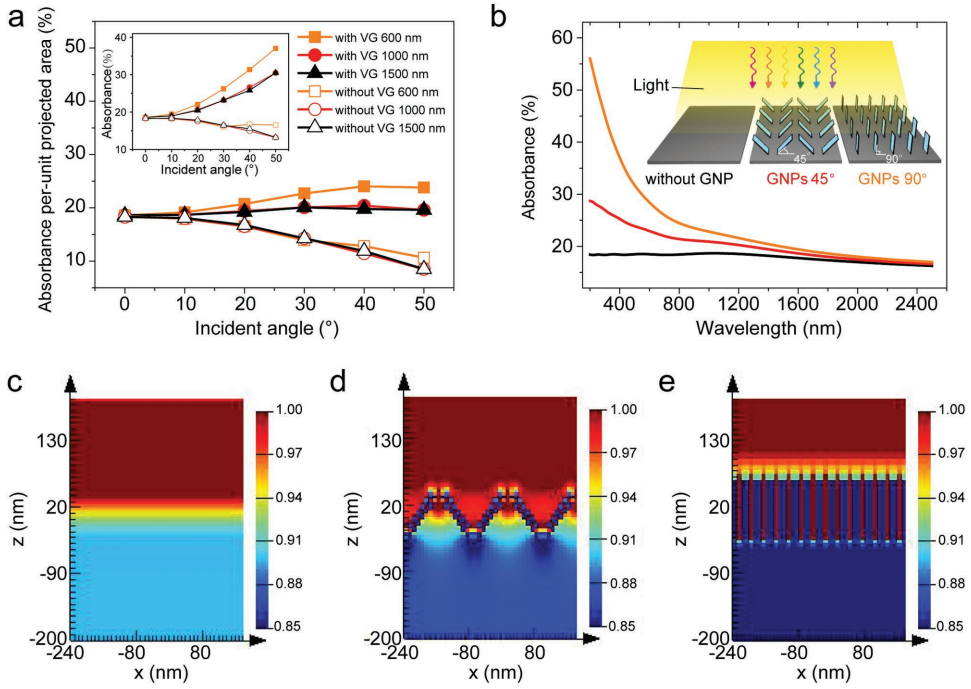

Figure 3. Calculated light absorption of h-G foam microstructures. a) Calculated absorption per-unit projected area of few layered graphene with and without GNP under varied incident angles at 600, 1000, and 1500 nm. Inset: The corresponding calculated absorption variation trend. b) Calculated absorption spectra of the three structures: few layered graphene without GNPs (black), with 45° GNPs (red) and with vertical GNPs (orange). Inset: Illustration of the calculation models. c–e) Calculated cross-sectional electric field distributions of partial of h-G foam at 600 nm. The three structures are graphene film without GNPs, with vertical GNPs and with 45° GNPs, respectively, from left to right. Color bar: 0.85–1.00, indicating the ratio of remaining electromagnetic energy to the total energy input.

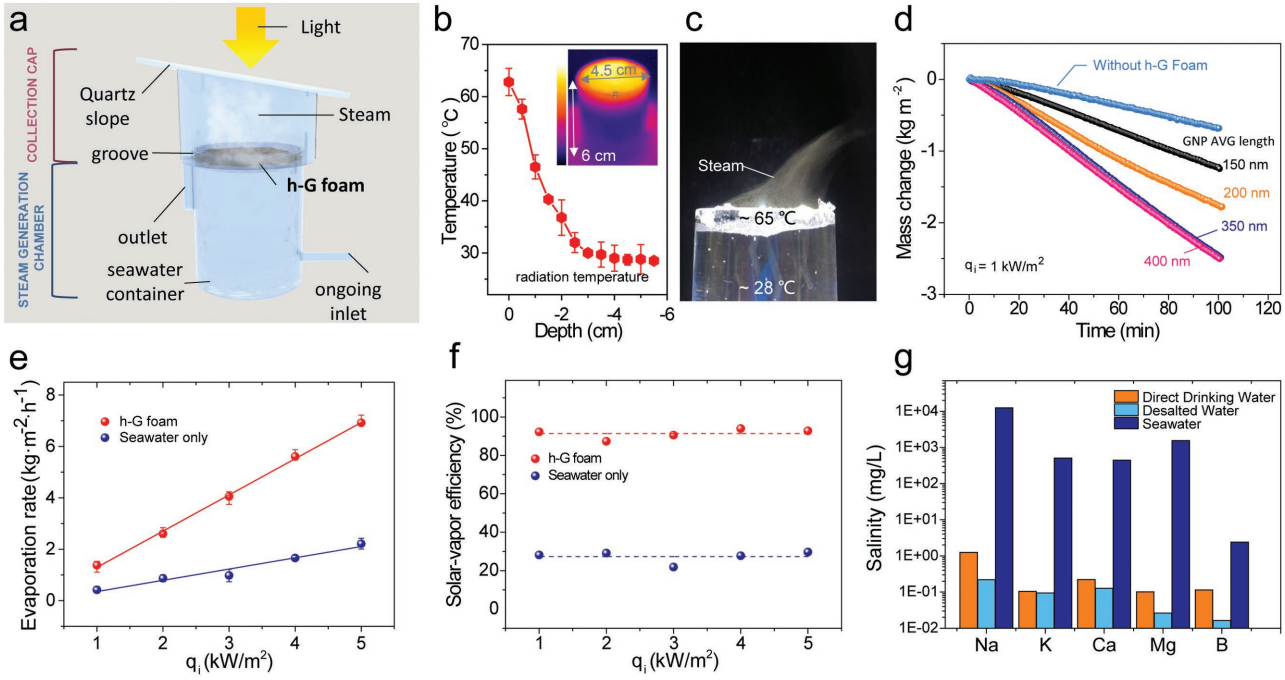

Figure 4. Performance of the hierarchical graphene foam for seawater desalination by solar–vapor generation. a) Structure of solar–vapor desalination unit used in experiment and the cross-section structure of steam generation part. b) Temperature distribution of the steam generation unit under solar illumination of 5 kW m^{-2}. The height of h-G foam surface was defined as depth of 0 cm. Inset: IR image of the corresponding unit. Color bar: 22–75 °C. c) Photo of water steam generated under solar illumination of 5 kW m^{-2}. d) Water evaporation performance under standard solar irradiation (1 kW m^{-2}) with and without heat localization absorbers. The absorbers are h-G foam samples with different GNP average (AVG) length (150, 200, 350, and 400 nm). e) Average evaporation rates of the h-G foam and seawater only under different solar illumination of 1–5 kW m^{-2}. f) Corresponding solar–vapor conversion efficiencies of (e). g) The measured concentrations of five primary ions in an actual seawater sample (from the Bohai Sea, Bohai Gulf, China; average salinity ≈2.75 wt %) before and after desalination, and direct drinking water sample.

temperature difference between the top and the bottom of the system has been observed after a 5 min irradiation under condensed solar illumination of 5 kW m^{-2} (Figure 4b). The heat was localized by h-G foam on the top of the liquid preventing the dissipating by thermal convection to a certain degree. There is visible steam generated at the same time (Figure 4c), which is in contrast to the seawater without h-G foam (Figure S9, Supporting Information). To determine the optimal sample, h-G foams with different length of GNPs were placed to the steam generation chamber for evaporation-time measurement. The corresponding mass changes with time under solar illumination of 1 kW m^{-2} are shown in Figure 4d, which are all subtracted the amount of natural evaporation (natural evaporation curve see Figure S10, Supporting Information). The curves show clearly that the weight loss per unit area with h-G foam on the top is much more than that without at the same illuminating duration, which equals to a higher evaporation rates. The longer GNPs in h-G foam, the faster the evaporation rates, which is consistent with the reflectance of these samples (Figure S11, Supporting Information). The evaporation rate of h-G foam with 400 nm GNP is 3.51 times faster than pure water at 1 kW m^{-2} and was chosen to be applied to the seawater desalination experiment. Note that few factors work cooperatively to influence the evaporation. Apart from minimizing reflectance rate, the structure of the nanoplates also provides plenty of vaporization nucleuses (further discussion in the Supporting Information).

In the case of seawater evaporation (seawater sample average salinity ≈2.75 wt%, from Bohai Sea, China), the average evaporation rates under different solar illumination of 1–5 kW m^{-2} were recorded (Figure 4e), which showed liner increase as the enhancement of illumination both in the cases with or without the h-G foams. The evaporation rate ratio of with/without h-G foam in seawater experiments is calculated to be 3.48, which shows a similar result to that of pure water. The solar–vapor conversion efficiency (η_{sv}) was calculated based on the required energy of vapor (v: evaporation rate and h_{LV}: enthalpy of sensible heat and phase change) and total solar energy input per unit time on the system ($\dot{q}_i$: illumination)[7]

$$\eta_{sv} = \frac{v h_{LV}}{\dot{q}_i} \quad (2)$$

The η_{sv} of h-G foam is around 91.4% while the η_{sv} of seawater only is 27.3% (Figure 4f). The relationship between the efficiency from measured data and the illumination increase is not obvious which could be ascribed to the measuring error instead of the energy loss. In spite of the improvable system design (e.g., concise system and heat insulation designs), insightful designs of the solar–thermal materials hold the key to enhance the solar–vapor efficiency. Several times of enhancement (varied from 1 to 3.5 times) of the steam generation using a variety of subtly designed materials were reported in different laboratories (Figure S13, Supporting Information),[1,3,5–8,13,14,27,28]

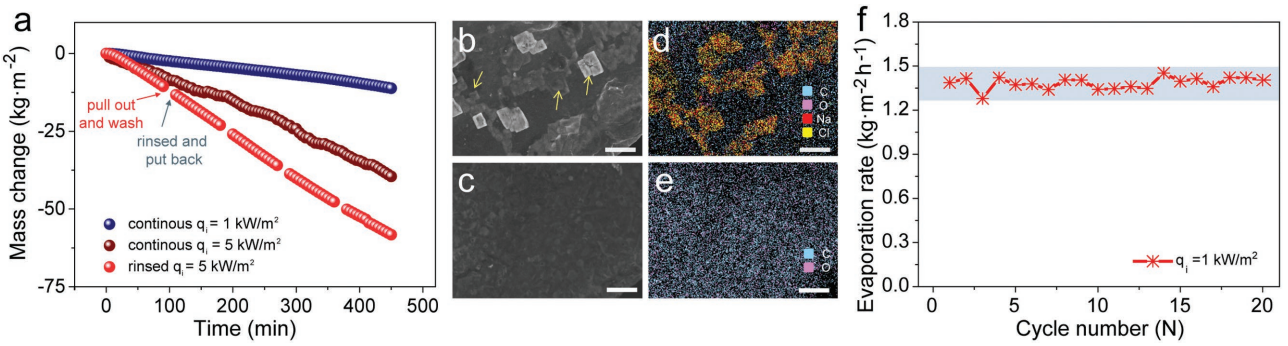

Figure 5. Effect of salt deposition and the desalination unit durability. a) Evaporation performance of long time continuous desalination under illumination of 1 kW m^{-2} (blue dots) and 5 kW m^{-2} (wine-red dots). And evaporation performance of recycled rinsed h-G foam for five times under 5 kW m^{-2} illumination (red dots). b) SEM images of salt deposition on the h-G foam frame used in desalination experiments for 240 min under solar illumination of 5 kW m^{-2}. Yellow arrows indicate the salt deposition position. c) SEM images of the same frame of h-G foam after washed by water. d,e) The energy dispersive X-ray spectroscopy mapping of the area corresponding to (b) and (c), respectively, showing the removal of salt. Scale bars in (a)–(d): 10 µm. f) Evaporation rates of the recycled rinsed h-G foam under solar illumination of 1 kW m^{-2}. Background blue bar indicates the solar–vapor conversion efficiency rage of 90–100%.

among which, h-G foam owns an outstanding solar–thermal conversion efficiency (≈3.51 times subtracted with the natural evaporation in dark).

To evaluate the quality of desalted water, concentrations of five primary ions, namely Na^+, K^+, Ca^{2+}, Mg^{2+}, B^{3+}, before and after desalination water samples as well as direct drinking water sample were collected by inductively coupled plasma optical emission spectrometer (Figure 4g). The ion concentration of desalted water was decreased to a fairly low level that is all below the concentration of direct drinking water samples. The salinity levels defined by World Health Organization is 103 mg L^{-1} which is much higher than our desalted water samples.[29] This h-G foam has a better desalination performance compared with conventional distillation method product whose salinity is 1–50 ppm.[30] The intriguing difference can be accounted for certain salt caught by h-G foam networks, which can be validated by the observation that some salt nucleates and grows on the h-G foam.

Durability is a very important issue for the practical use of the h-G foam in desalination. The conventional desalination is plagued by many drawbacks, such as erosion and blockage of the materials of heat exchangers and units.[31] Obviously, the h-G foam avoids the corrosion problem due to the excellent chemical stability of graphene. The primary structure of h-G foam's holes (>50 µm) is free from the channel blockage by salt under 1 kW m^{-2} for 7.5 h and keeping the high solar–vapor conversion efficiency (**Figure 5**a, blue dots). After long-term operations under 5 kW m^{-2}, the evaporation rates are below the expectation based on the short-term measurement (Figure 5a, wine red dots). However, this issue can be overcome simply by cooling and washing the material for several times (Figure 5a, red dots). Meanwhile, the salt deposited on the frame (Figure 5b–d) would affect the desalination performance under high illumination intensity, but the salts sitting on h-G foam are removable by dip rinsing (Figure 5e,f). Figure 5f shows the cycle performance of h-G foam under 1 kW m^{-2} for 20 cycles with each sustained for 1.5 h keeping the high evaporation rate around 1.4 kg m^{-2} h^{-1}, indicating that h-G foam is easily reused.

In conclusion, h-G foam was prepared by a scalable PECVD method, where light absorption was significantly improved by the GNPs anchoring on the surface of foam skeleton. Considering that the available solar energy in the field highly depends on location, time, and weather, these GNPs structure was also designed to make the light absorption of the h-G foam independent on incident angle. Therefore, the solar–thermal conversion efficiency was dramatically enhanced by h-G foam (≈93.4%) which is much superior to that of traditional graphene foams and other carbon-based solar–thermal materials. Additionally, as one example, h-G foam was used as a light absorber and efficient heater in a solar-driven seawater desalination system. The solar–vapor conversion efficiency exceeds 90% with excellent durability, recycling performance, and anticorrosion property. The as-presented h-G foam design may open up a new way for designing solar–thermal conversion material for various fields such as water remediation and desalination.

Experimental Section

Growth of Hierarchical Graphene Foam: In a typical procedure, commercial Ni foams with a thickness of 1.6 mm were cut into size of 5.5 × 9 cm^2. After carefully cleaned, substrates were placed in the hot center of the furnace. The plasma generator was made up of Cu coil and radio frequency power (RFG-500 radio frequency power, Tailong Electronics). Initially, the system was evacuated to a base pressure of 0.1 Pa and heated to 700 °C. After annealed with 100 sccm hydrogen for 10–30 min, 7 sccm methane was introduced in the system with a pressure of 15 Pa, and plasma generator was turned on with a power of 150 W to generate methane plasma. Afterward, the deposition lasted for 0.17–3 h, followed by fast cooling process to room temperature (see the Supporting Information for more details).

Characterization: SEM characterizations were done using a Hitachi S-4800 with 5–30 kV acceleration voltage. The IR-image of temperature profile was obtained by an FLUKE Ti 10 Infrared Camera. Raman spectra were measured using a Jobin Yvon LabRAM HR 800UV with a 25 mW, 514.5 nm laser. Selected area electron diffraction measurements were performed using an FEI Tecnai F20 with acceleration voltage 200 kV. The transmittance and reflectance was measured by UV–vis–NIR Perkin Elmer Lambda 950 spectrophotometer. The light source using in experiments is solar simulator produced by SAN-EI ELECTRIC

XES-160S1. The concentration of ions was collected by Inductively Coupled Plasma-Optical Emission Spectrometer, PROFILE SPEC, Teledyne Leeman Labs.

Supporting Information

Supporting Information is available from the Wiley Online Library or from the author.

Acknowledgements

H.R., M.T., and B.G. contributed equally to this work. The authors acknowledge financial support from the National Natural Science Foundation of China (Grant Nos. 51520105003, 51432002, 21222303, and 51362029) and the Ministry of Science and Technology of China (Grant Nos. 2014CB932500, 2013CB932603, and 2012CB933404), the National Program for Support of Top-Notch Young Professionals, and Beijing Municipal Science and Technology Commission (Z161100002116002).

Conflict of Interest

The authors declare no conflict of interest.

Keywords

desalination, graphene, hierarchical foams, solar–thermal conversion

Received: May 9, 2017
Revised: July 1, 2017
Published online: August 18, 2017

[1] L. Zhou, Y. Tan, J. Wang, W. Xu, Y. Yuan, W. Cai, S. Zhu, J. Zhu, *Nat. Photonics* **2016**, *10*, 393.
[2] K. Bae, G. Kang, S. K. Cho, W. Park, K. Kim, W. J. Padilla, *Nat. Commun.* **2015**, *6*, 10103.
[3] L. Zhou, Y. Tan, D. Ji, B. Zhu, P. Zhang, J. Xu, Q. Gan, Z. Yu, J. Zhu, *Sci. Adv.* **2016**, *2*, e1501227.
[4] Z. Hua, B. Li, L. Li, X. Yin, K. Chen, W. Wang, *J. Phys. Chem. C* **2017**, *121*, 60.
[5] J. Wang, Y. Li, L. Deng, N. Wei, Y. Weng, S. Dong, D. Qi, J. Qiu, X. Chen, T. Wu, *Adv. Mater.* **2017**, *29*, 1603730.
[6] Q. Jiang, L. Tian, K.-K. Liu, S. Tadepalli, R. Raliya, P. Biswas, R. R. Naik, S. Singamaneni, *Adv. Mater.* **2016**, *28*, 9400.
[7] H. Ghasemi, G. Ni, A. M. Marconnet, J. Loomis, S. Yerci, N. Miljkovic, G. Chen, *Nat. Commun.* **2014**, *5*, 4449.
[8] Y. Ito, Y. Tanabe, J. Han, T. Fujita, K. Tanigaki, M. Chen, *Adv. Mater.* **2015**, *27*, 4302.
[9] Q. Bao, K. P. Loh, *ACS Nano* **2012**, *6*, 3677.
[10] Y. Shen, A. G. Skirtach, T. Seki, S. Yagai, H. Li, H. Möhwald, T. Nakanishi, *J. Am. Chem. Soc.* **2010**, *132*, 8566.
[11] D.-K. Lim, A. Barhoumi, R. G. Wylie, G. Reznor, R. S. Langer, D. S. Kohane, *Nano Lett.* **2013**, *13*, 4075.
[12] M. A. Shannon, P. W. Bohn, M. Elimelech, J. G. Georgiadis, B. J. Mariñas, A. M. Mayes, *Nature* **2008**, *452*, 301.
[13] Y. Wang, L. Zhang, P. Wang, *ACS Sustainable Chem. Eng.* **2016**, *4*, 1223.
[14] X. Hu, W. Xu, L. Zhou, Y. Tan, Y. Wang, S. Zhu, J. Zhu, *Adv. Mater.* **2017**, *29*, 1604031.
[15] Y. Ma, Y. Chen, *Natl. Sci. Rev.* **2015**, *2*, 40.
[16] Z. Chen, W. Ren, L. Gao, B. Liu, S. Pei, H.-M. Cheng, *Nat. Mater.* **2011**, *10*, 424.
[17] H. Bi, I.-W. Chen, T. Lin, F. Huang, *Adv. Mater.* **2015**, *27*, 5943.
[18] K. Liu, Y.-M. Chen, G. M. Policastro, M. L. Becker, Y. Zhu, *ACS Nano* **2015**, *9*, 6041.
[19] L. Shi, K. Chen, R. Du, A. Bachmatiuk, M. H. Rümmeli, K. Xie, Y. Huang, Y. Zhang, Z. Liu, *J. Am. Chem. Soc.* **2016**, *138*, 6360.
[20] M. Liu, X. Yin, E. Ulin-Avila, B. Geng, T. Zentgraf, L. Ju, F. Wang, X. Zhang, *Nature* **2011**, *474*, 64.
[21] M. Zhu, J. Wang, B. C. Holloway, R. A. Outlaw, X. Zhao, K. Hou, V. Shutthanandan, D. M. Manos, *Carbon* **2007**, *45*, 2229.
[22] G. Sato, T. Morio, T. Kato, R. Hatakeyama, *Jpn. J. Appl. Phys.* **2006**, *45*, 5210.
[23] S. Kurita, A. Yoshimura, H. Kawamoto, T. Uchida, K. Kojima, M. Tachibana, *J. Appl. Phys.* **2005**, *97*, 104320.
[24] D. K. Roper, W. Ahn, M. Hoepfner, *J. Phys. Chem. C* **2007**, *111*, 3636.
[25] C. M. Hessel, V. P. Pattani, M. Rasch, M. G. Panthani, B. Koo, J. W. Tunnell, B. A. Korgel, *Nano Lett.* **2011**, *11*, 2560.
[26] H. K. Raut, V. A. Ganesh, A. S. Nair, S. Ramakrishna, *Energy Environ. Sci.* **2011**, *4*, 3779.
[27] L. Zhang, B. Tang, J. Wu, R. Li, P. Wang, *Adv. Mater.* **2015**, *27*, 4889.
[28] Y. Liu, S. Yu, R. Feng, A. Bernard, Y. Liu, Y. Zhang, H. Duan, W. Shang, P. Tao, C. Song, T. Deng, *Adv. Mater.* **2015**, *27*, 2768.
[29] *World Health Organization, Guidelines for Drinking-Water Quality*. Fourth Edition, World Health Organization, Geneva, Switzerland **2011**.
[30] S. P. Surwade, S. N. Smirnov, I. V. Vlassiouk, R. R. Unocic, G. M. Veith, S. Dai, S. M. Mahurin, *Nat. Nanotechnol.* **2015**, *10*, 459.
[31] X. Wang, K. C. Ng, *Appl. Therm. Eng.* **2005**, *25*, 2780.